Effects of Surface Chemistry on the Generation of Reactive Oxygen Species by Copper Nanoparticles

Miao Shi,[†] Hyun Soo Kwon,[†] Zhenmeng Peng,[†] Alison Elder,[‡] and Hong Yang[†,§,*]

[†]Department of Chemical Engineering, University of Rochester, Gavett Hall 206, Rochester, New York 14627, United States and [‡]Department of Environmental Medicine, University of Rochester, 575 Elmwood Avenue, Rochester, New York 14642, United States. [§]Present address: Department of Chemical and Biomolecular Engineering, University of Illinois at Urbana—Champaign, 114 Roger Adams Laboratory, MC-712, 600 S. Mathews Avenue, Urbana, IL 61801.

ABSTRACT

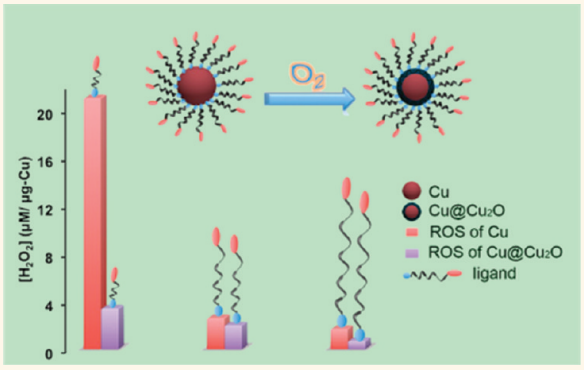

Mercaptocarboxylic acids with different carbon chain lengths were used for stabilizing uniform 15 nm copper nanoparticles. The effects of surface chemistry such as ligand type and surface oxidation on the reactive oxygen species (ROS) generated by the copper nanoparticles were examined. Transmission electron microscopy (TEM), powder X-ray diffraction (PXRD), UV—vis spectroscopy, and an acellular ROS assay show that ROS generation is closely related to the surface oxidation of copper nanoparticles. It was found that the copper nanoparticles with longer chain ligands had surfaces that were better protected from oxidation and a corresponding lower ROS generating capacity than did particles with shorter chain ligands. Conversely, the copper nanoparticles with greater surface oxidation also had higher ROS generating capacity.

KEYWORDS: copper nanoparticles · ROS · oxidation · surface chemistry · mercaptocarboxylic acids

With the increasing commercial and therapeutic applications of engineered nanoparticles, study of the potential adverse effects of these materials on public and environmental health becomes an important research topic.[1−9] Both short- and long-term *in vitro*[4,6,10,11] and *in vivo*[12,13] studies have been carried out with many nanoparticles.[14,15] There is a growing concern about the use of copper-containing nanoparticles, specifically, as they are used in commercial products such as inks, lubricants, and coatings, and these materials can be cytotoxic.[8,16] The bactericidal and fungicidal properties of copper nanoparticles are known.[17−19] Rakhmetova *et al.* found that copper nanoparticles prepared by a high-temperature method and modified with a variety of agents showed potential for enhancing wound healing.[20] These applications may lead to increased exposure in human and environmental receptor species, so it is important to learn more about the mechanisms of toxicity of copper and copper oxide nanoparticles.

Oxidative stress is important when examining the mechanism of the toxicity of copper-based nanomaterials. For instance, when cells were exposed to copper oxide nanoparticles, the level of 8-isoprostane and the ratio between oxidized and total glutathione in cells increased significantly, indicating a high level of oxidative stress in cells.[21] Midander *et al.* also showed that copper nanoparticles were much more toxic than micro-sized particles in terms of DNA damage and cytotoxicity *in vitro*. Though nanoparticles released more copper than the micrometer-sized particles, the released fraction did not contribute significantly toward cytotoxicity when compared to particles themselves.[22] Likewise, other *in vitro* studies using cultured lung epithelial cells have shown that exposure to copper containing nanoparticles led to increased intracellular reactive oxygen species (ROS) formation, oxidative DNA damage, and cell death.[8,10] Rushton *et al.*[9] showed that the native oxidant potential of metallic copper nanoparticle powders—as determined *via* oxidation of dichlorodihydrofluorescein (DCFH) and other methods—correlated well with oxidant stress-related inflammatory mediator production in cultured cells and with their acute *in vivo* inflammatory

* Address correspondence to hy66@illinois.edu.

Received for review October 18, 2011 and accepted February 28, 2012.

Published online March 05, 2012
10.1021/nn300445d

© 2012 American Chemical Society

potency. In spite of these studies, there are many unknowns regarding the toxicity of copper particles.

It is essential to develop approaches to control surface chemistry to better understand the origins of nanoparticle-induced toxicity, as subtle differences in surface properties can dramatically change biological responses.[23−25] In this work, we study the ROS generating capacity of uniform copper nanoparticles with different capping ligands to better understand the relationship between nanoparticle physicochemical properties and their toxicological potential as reflected by ROS generation in an acellular assay. Three mercaptocarboxylic acids with different carbon chain lengths were used for surface modification as they have been shown to provide good colloidal stability for various nanoparticles.[26−28]

RESULTS AND DISCUSSION

The copper nanoparticles used in this study were made in oleylamine under argon and characterized by TEM, PXRD, and ATR-IR techniques. Figure 1 shows the TEM micrographs of as-synthesized copper nanoparticles. The particles are spherical and have an average diameter of 15 nm (Figure 1a). In this synthesis, oleylamine provided good stability, as no obvious aggregated or agglomerated structures were observed. The TEM micrograph shows that the nanoparticle was crystalline with only limited surface oxidation (Figure 1b). The lattice distance of the nanoparticle was determined to be 0.21 nm, and the angle between those two planes was 72°. These results indicated that the lattices were (111) planes of a face-centered cubic (fcc) copper metal.

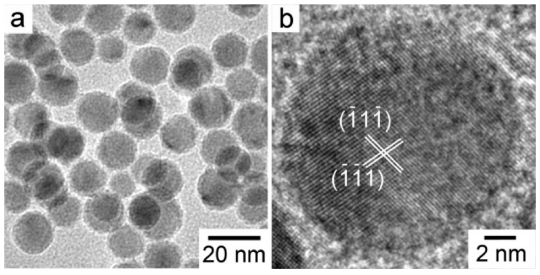

Figure 1. (a) TEM and (b) HR-TEM micrographs of as-synthesized copper nanoparticles.

Figure 2 shows the TEM micrographs of these copper nanoparticles after surface modification with 8-mercaptooctanoic acid (MOA), 12-mercaptododecanoic acid (MDA), and 16-mercaptohexadecanoic acid (MHA). The modification was carried out through ligand exchange overnight under an argon atmosphere. The size and morphology of nanoparticles remained intact, though the particles slightly agglomerated upon drying on the TEM grids.

After surface treatment, copper nanoparticles were readily dispersible in water, indicating that thiolated functional groups have strong affinity to copper nanoparticles while carboxylic acids facilitate aqueous dispersibility. Figure 3a,b shows the photographs of dispersions of copper nanoparticles before and after the surface modification, respectively. Before the ligand exchange, the nanoparticles dispersed exclusively in the organic phase (Figure 3a). They were transferred into the aqueous phase after surface modification (Figure 3b). Figure 3c,d shows TEM micrographs of the monodispersed copper nanoparticles after surface modification with MOA (Cu-MOA) and MDA (Cu-MDA), respectively. The size and morphology remained the same.

The crystalline structures of these copper nanoparticles were examined using PXRD (Figure 4). All samples had the three main diffraction peaks that correspond to (111), (200), and (220) planes of fcc phase copper. For MOA-modified copper nanoparticles, an additional broad peak was apparent, centered around 36.5° 2θ and indicated by an arrow in Figure 4. This peak was from the (111) plane of Cu_2O. As copper metal readily reacts with oxygen, the oxidation likely occurred during the PXRD measurement when the specimen was exposed to air. Copper nanoparticles modified with MDA and MHA had very similar peaks at around 36.5° 2θ in their corresponding PXRD patterns, though the intensity was either much weaker than that with MOA or not readily detectable. This observation indicates that copper nanoparticles were oxidized more slowly when modified with MDA and MHA than with MOA, suggesting that the ligands with long

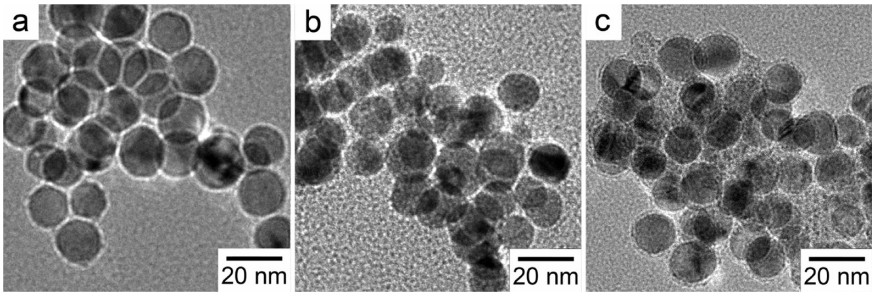

Figure 2. TEM micrographs of copper nanoparticles dispersed in ethanol after surface modification with (a) MOA, (b) MDA, and (c) MHA.

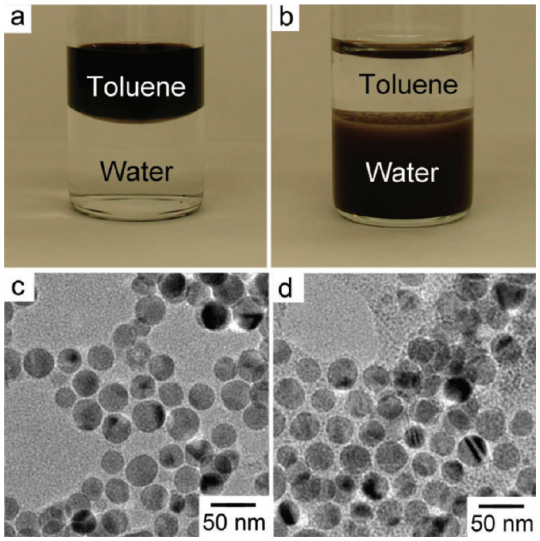

Figure 3. Photographs of copper nanoparticles (a) in toluene before surface modification and (b) in water after surface modification with MOA; and TEM micrographs of copper nanoparticles dispersed in water after surface modification with (c) MOA and (d) MDA.

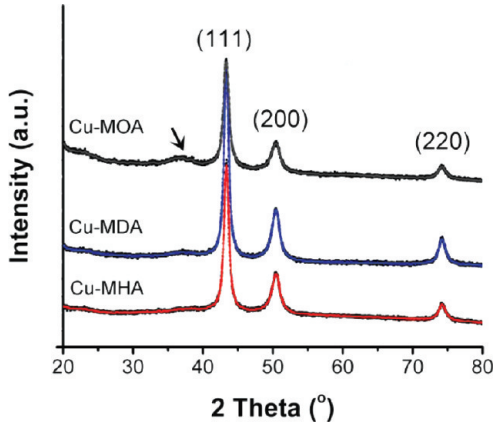

Figure 4. PXRD spectra of copper nanoparticles after surface modification with MOA, MDA, and MHA.

carbon chains could protect the copper surface from oxidation better than those with short chains.

ATR-IR spectra were used to study the ligands on the copper nanoparticles after the modifications (Figure 5). The IR spectrum of as-synthesized copper nanoparticles contains peaks at 2916, 2849, 1647, and 1581 cm^{-1} (Figure 5a). These IR absorptions were from oleylamine, which has the C−H stretch modes at 2920 and 2850 cm^{-1}, ν(C−H) bond adjacent to the C═C bond at 3006 cm^{-1}, C═C stretch at 1647 cm^{-1}, and N−H scissoring mode at 1593 cm^{-1} (Figure S1a in the Supporting Information).[26,29] After surface modification with MOA, IR peaks appeared at 1710, 1560, and 1420 cm^{-1}, which was attributed to C═O and COO−. Compared to those of pure MOA, the corresponding peaks shifted slightly from 1703 to 1710 cm^{-1} and from 1426 to 1420 cm^{-1} (Figure S1b). These changes are

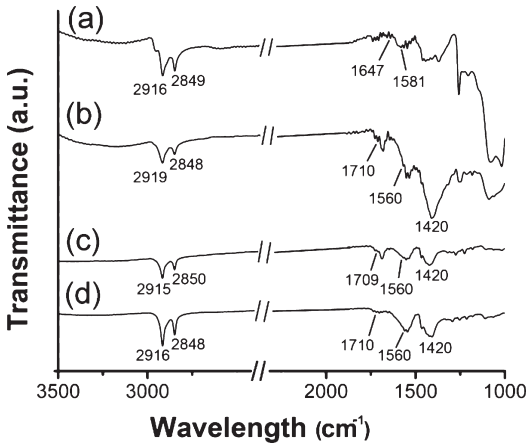

Figure 5. ATR-IR spectra of copper nanoparticles: (a) as-synthesized and after surface modifications with (b) MOA, (c) MDA, and (d) MHA.

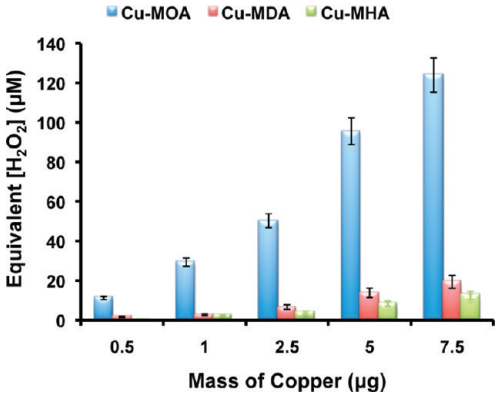

Figure 6. ROS generated by copper nanoparticles after surface modification with MOA, MDA, and MHA. (All data were mean values plus/minus standard deviations calculated from three independent tests.)

likely related to the interaction between copper and the thiol functional group. We also observed that the intensity of the peak around 1710 cm^{-1} decreased, while the intensity of those at 1420 and 1560 cm^{-1} increased, indicating the deprotonation of carboxylic acid.[27] The peaks related to oleylamine at 1647 and 1581 cm^{-1} disappeared or were reduced substantially, indicating the large degree of surface modifications. The ATR-IR spectra of MDA and MHA-modified copper nanoparticles revealed very similar results to those of MOA (Figure 5c,d).

The ROS generating capacities of these three copper nanoparticle types were measured and shown in Figure 6. All particles demonstrated dose-dependent increases in ROS activity. The Cu-MOA exhibited a high level of ROS capacity, which was equivalent to about 21 μM H_2O_2/μg Cu, while ROS generating capacities were 2.6 μM H_2O_2/μg Cu for Cu-MDA and 1.7 μM H_2O_2/μg Cu for Cu-MHA. These results indicate that, with the increasing chain lengths on the nanoparticle surface, ROS generating capacities greatly decreased.

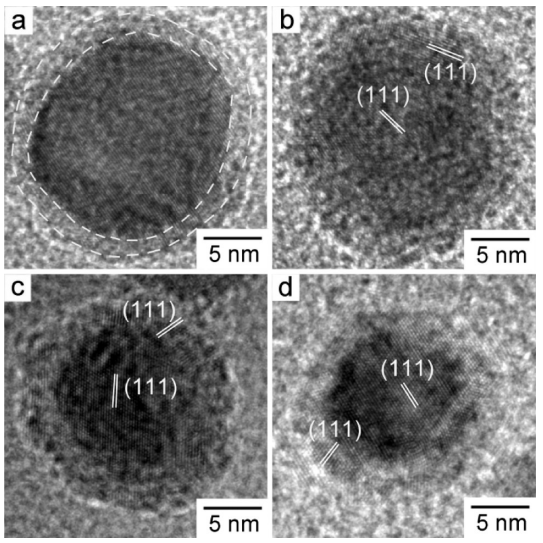

Figure 7. HR-TEM micrographs of as-synthesized copper nanoparticles after exposure to air for (a) 30 min, (b) 2 h, (c) 5 h, and (d) 1 day.

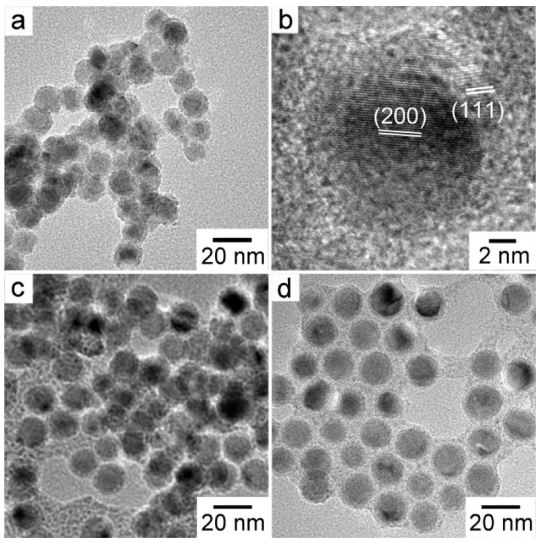

Figure 8. TEM of oxidized copper nanoparticles after surface modification with (a,b) MOA, (c) MDA, and (d) MHA.

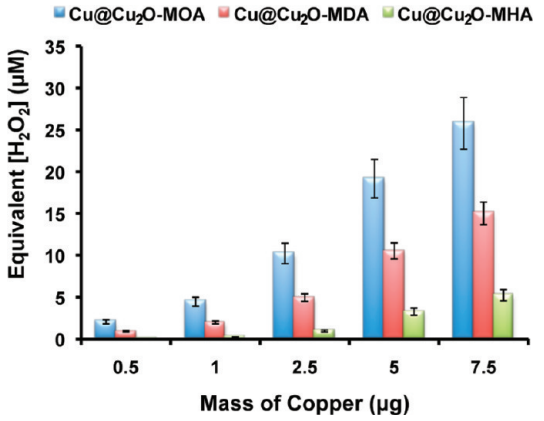

Figure 9. ROS assay results of surface-modified copper nanoparticles after oxidation for 20 h under ambient air. (All data were mean values plus/minus standard deviations calculated from three independent tests.)

Copper nanoparticles have been known to generate ROS, though the mechanism is not clear.[30] As redox reactivity is important during the generation of ROS and copper is quite reactive with oxygen, we carried out controlled experiments by oxidizing these three copper samples under ambient air conditions to directly study the effect of surface oxidation on ROS generation.

Oxidation of as-made copper nanoparticles, which was carried out in toluene in an open vial under ambient conditions, was used to study resultant structural and compositional changes. Figure 7 shows the TEM micrographs of copper nanoparticles made in oleylamine after exposure to air for up to 1 day. A thin oxide layer was observed after exposure for 30 min, and no obvious long-range lattice formed in the oxide layer. After exposure for 2 h, a low contrast layer with a thickness of about 2.5 nm developed on the outer surface of the nanoparticles. This oxide layer grew to about 3.5 nm in thickness after 5 h. After 1 day, the thickness of the oxide layer was measured to be about 3.6 nm. HR-TEM study confirmed that the inner core was still copper metal with a lattice spacing of 0.20 nm for the (111) plane, and the outside layer had a cubic phase cuprous structure with a lattice spacing of 0.24 nm for the (111) plane.

Oxidation of copper nanoparticles involves a fast reaction of converting Cu to CuO_x ($x \sim 0.67$) with Cu_2O structure and then a slow and continuous oxidation with x changing from 0.67 to ~1 when the reaction temperature increases from 298 to 673 K.[31] In this study, the temperature was kept at room temperature, so the observed oxide phase was largely Cu_2O with no change in either the oxidation state or layer thickness after 1 day. Even after air exposure for 17 days, the oxide layer remained around 3.6 nm. The oxidation rate is sufficiently slow that any visible changes in layer thickness are not observable up to 17 days, though the oxide layer may keep growing over months or even years.

On the basis of this observation, we further studied the oxidation of the three surface-modified copper samples under ambient air for 20 h. Figure 8 shows the TEM micrographs of the three copper nanoparticles after air exposure. For Cu-MOA, a thin layer with low contrast was observed on the surface of the nanoparticles. In comparison with as-made nanoparticles (Figure 2), the morphology changed slightly and the surface became rough. However, there is no significant change in particle size overall because the oxide layer is thin. The HR-TEM micrograph (Figure 8b) shows that the inner core of the particles had lattice spacing of 0.18 nm, which indicates the (200) plane of fcc copper metal. The low contrast outer layer, which

TABLE 1. Results of ROS Assay Using $CuCl_2$ Solutions[a]

amount of $CuCl_2$ per Cu (μg)	fluorescent intensity (au)	equiv of $[H_2O_2]$ (μM)	equiv of $[H_2O_2]$ after subtracting the blank (μM)
4	21	0.53	0.35
8	21.5	0.70	0.30
16	17	0.35	0.05
24	12	0.30	0.10

[a] The blank is a mixture of DCFH and HRP in the buffer solution.

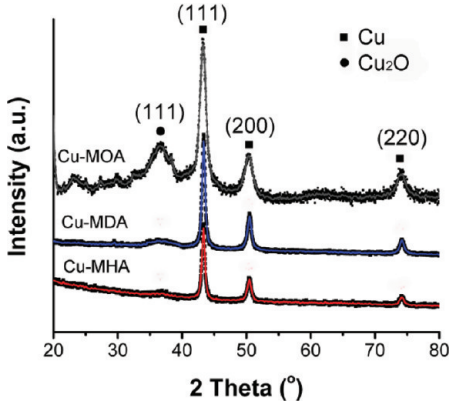

Figure 10. PXRD of the three surface-modified copper nanoparticles after oxidation for 20 h under ambient air.

had an average thickness of 3 nm, had a lattice spacing of 0.24 nm, corresponding to the (111) plane of Cu_2O. Thin oxide layers were also observed for the oxidized Cu-MDA and Cu-MHA samples (Figure 8c,d and Figure S3). The thickness, however, was less than that of the Cu-MOA sample and difficult to image under high-resolution TEM, as shown in Figure S3. The thickness for oxidized Cu-MDA is about 1.1 nm; it is hard to measure for oxidized Cu-MHA, but it is less than 1 nm. The nanoparticle surface became slightly rough for these two samples, although the morphology did not change much. Overall, the Cu-MOA sample was oxidized the most and had the thickest oxide layer.

The ROS generating capacities of the oxidized copper samples are shown in Figure 9. The oxidized copper nanoparticles had lower equivalent $[H_2O_2]$ than the corresponding as-made ones (Figure 6). The equivalent $[H_2O_2]$ for the Cu-MOA sample decreased to 3.4 μM H_2O_2/μg Cu. This value is about 80% less than without oxidation. Thus, the surface oxide appears to dramatically reduce the ROS generating capacity of the copper nanoparticles. The equivalent $[H_2O_2]$ fell to 2 μM/μg Cu for Cu-MDA and 0.7 μM/μg Cu for Cu-MHA after surface oxidation. The same trend in ROS generating capacity, specifically a decrease with the increasing chain length of surface molecules, was observed after oxidation of the nanoparticle surface.

Table 1 shows the results from the ROS assay using $CuCl_2$ solutions with amount of Cu up to 24 μg. It is clear that the soluble species of Cu did not contribute to ROS generation, suggesting that the ROS response should be attributed to the Cu nanoparticles.

TABLE 2. Cu_2O Domain Thickness of Oxidized Cu Nanoparticles with Different Surface Ligands

sample	*B* (rad)	cos θ	*t* (nm)
Cu@Cu_2O-MOA	0.052	0.826	3.1
Cu@Cu_2O-MDA	0.079	0.826	2.1
Cu@Cu_2O-MHA	0.087	0.826	1.9

PXRD was carried out for the three air-oxidized samples to examine the structure of the surface oxide (Figure 10). These samples had similar XRD patterns. Besides copper metal, a new peak at 36.5° 2θ, which corresponds to the (111) plane of Cu_2O, appeared. This peak was noticeably broader than that for copper, indicating the low crystallinity and/or small domain size of the oxide layers. The mean Cu_2O domain thickness was estimated according to Scherrer's equation:

$$t = 0.88\lambda/B\cos\theta$$

where *t* is the mean domain size, *B* is the value of full width of half-maximum (fwhm) of the diffraction peak, and λ is the X-ray wavelength and equal to 1.5405 Å in this case. The results are summarized in Table 2.

The surface-oxidized Cu-MOA had the narrowest Cu_2O diffraction peak and thus the thickest oxide layer among the three samples, while the Cu-MHA had the thinnest oxide layer. Direct measurement of the thickness of oxide layers was carried out using TEM. While the oxide layer thickness for Cu-MOA was about 3 nm after the exposure in air for 20 h (Figure 8), the thickness for Cu-MDA and Cu-MHA was around 1 nm after the same oxidation procedure. These analyses indicate that copper nanoparticles modified with MOA were more easily oxidized than the other two, potentially because MOA has the shortest carbon chain length and is less likely than MDA and MHA molecules to form tightly packed hydrophobic layers on the metal particle surfaces. This observation is consistent with previous reports that longer carbon chain thiol molecules on the surface improved the oxidation resistance of copper nanoparticles.[32] Our results also indicate that the copper nanoparticles that were readily oxidized in air also had high ROS generating capacity.

Previous studies showed that the surface oxidation of metals eventually stopped after the oxide layer reached a critical thickness at low temperature.[33] For copper, this thickness was reported to be 13 nm at room temperature. Oxygen adsorbed at the surface of nanoparticles, resulting in a contact potential difference between metal and adsorbed oxygen, with copper ions moving through the oxide.[33] Slow growth of a copper oxide layer over a year was also observed.[34] It is likely that the diffusion of oxygen atoms to the surface

of copper nanoparticles is the critical step and can be inhibited in part by surface ligands. With the mercaptocarboxylic group, oxygen diffusion to the nanoparticle surface was greatly hindered because of the surface coverage by the ligands. Thus, less oxygen reached the surface. According to the oxidation theory of Cabrera *et al.*,[33] when metal is oxidized, oxygen first adsorbs on the metal surface and is then converted into ions, creating a potential difference between metal and adsorbed oxygen. The metal ions are then attracted to the surface to form bonds with oxygen, resulting in the growth of an oxide layer. The electrostatic potential is independent of the thickness of the oxide layer but dependent on the pressure or concentration of oxygen. The electrostatic field between oxygen and metal is proportional to this potential and inversely proportional to the oxide thickness, so when less oxygen adsorbs on the surface and/or the oxide layer thickens, the field will not be strong enough to attract metal ions and the growth of the oxide will slow down or even stop. We noted from our studies that the oxidation of copper nanoparticles occurred rapidly upon exposure to air and the formed oxide layer can protect the nanoparticles from further oxidation at room temperature (Figure 7). As the oxide layer formed, the ROS generating capacity of the copper nanoparticles was reduced.

Surface plasmon resonance has been used to study the oxidation kinetics of metal nanoparticles. Chan *et al.* found that the presence of copper oxide significantly affected the surface plasmonic property of copper nanoparticles.[35] The surface plasma peak of copper underwent a red shift, and the intensity decreased when a layer of copper oxide (up to 6 nm) formed. Others also observed this phenomenon.[32,36,37] We proposed that there is a relationship between the growth of the oxide layer and the decay in SPR intensity, thus surface plasmon resonance provides a way to study the growth of a copper oxide surface layer under controlled conditions in terms of the decay in SPR intensity.

We carried out a series of studies of the decay in SPR intensity of surface-modified copper nanoparticles using UV–vis spectroscopy. Oxidation under air is a relatively slow process, so this oxidation process was facilitated by bubbling compressed air through the dispersions of surface-modified copper nanoparticles at a rate of ~16 cm^3/min. Figure S2 shows the resulting UV–vis spectra. Copper nanoparticles exhibited a well-defined peak in the visible range, though the position may change with the size of the nanoparticles.[38] For the 15 nm copper nanoparticles, the surface plasmon absorption occurred at around 580 nm, which is consistent with previous reports.[36] After oxidation for 35 min, the UV–vis spectra exhibited a red shift and the intensity decreased. The peak at 350 nm, which is characteristic for Cu_2O,[39,40] became much broader for Cu-MDA and Cu-MHA than that for Cu-MOA. By fitting the intensity of these peaks around 580 nm as a function of reaction time, we obtained the rates of the decay in SPR intensity. The reaction appeared to be pseudo-first-order and could be fit according to the following rate equation:

$$\ln C_A = \ln C_{Ao} - kt$$

where C_{Ao} is the initial SPR intensity, C_A is the SPR intensity at time t, and k is the rate constant. On the basis of this equation, we obtained the rate constants for the decay in SPR intensity of copper nanoparticles: 1.3×10^{-2} s^{-1} for Cu-MOA, 1.9×10^{-3} s^{-1} for Cu-MDA, and 1.4×10^{-3} s^{-1} for Cu-MHA. Cu-MOA was nearly 7 times as active as Cu-MDA and 9 times as active as Cu-MHA. The ROS generation capacity of Cu-MOA was about 6.5 times as much as that of Cu-MDA and 10 times as much as that of Cu-MHA. The decay in SPR intensity may indicate the rate of the surface oxidation of copper nanoparticles. It suggests that the ROS generation capacity of copper nanoparticles should be closely associated with the ability of oxygen to access the surface layer and with the surface composition.

CONCLUSION

Well-characterized uniform copper nanoparticles with different surface ligands provide a good platform for studying the effects of surface chemistry on ROS generated by the metal species. Mercaptocarboxylic ligands with different chain lengths were used for surface modification. ROS assays indicate that long carbon chain molecules greatly reduce ROS generation by the copper nanoparticles. Convergent evidence from TEM, XRD, and UV–vis analyses shows that the surface-capping ligand and composition greatly affect the surface oxidation reactivity of copper nanoparticles, resulting in different ROS responses. The approach developed in this work to systematically alter surface chemistry could also be applied more generally to the investigation of oxidative stress-related toxicological mechanisms of response to nanoparticles.

MATERIALS AND METHODS

Synthesis of Copper Nanoparticles. The preparation of copper nanoparticles followed a modified procedure.[41] Briefly, 0.1 mg of copper acetylacetonate (Aldrich, 99.99%, 0.4 mmol) was dissolved in 10 mL of oleylamine (Sigma-Aldrich, 70%) in a 25 mL flask. The solution was degassed for 5 min and subsequently protected under a flow of argon gas. The reaction mixture was heated to 230 °C at a rate of 5 °C/min by a heating

mantle while being magnetically stirred and then kept at 230 °C for 2.5 h. After the reaction, the product was cooled to room temperature. The subsequent washing and surface modification processes were conducted in an argon-filled glovebox. All solvents used were degassed with argon for 20 min. The product was washed with toluene and ethanol (v/v = 1:15) and centrifuged at 7500 rpm for 5 min. This washing process was repeated three times.

Procedure for Surface Modification. 8-Mercaptooctanoic acid (MOA, Sigma-Aldrich), 12-mercaptododecanoic acid (MDA, Sigma-Aldrich), and 16-mercaptohexadecanoic acid (MHA, Sigma-Aldrich) were used as the ligands. In general, 8 μL of MOA (0.05 mM), 0.011 g of MDA (0.05 mM), or 0.013 g of MHA (0.05 mM) was dissolved in 7 mL of ethanol separately. The above ligands in ethanol were then added into three separate vials with about 5−7 mg of as-synthesized copper nanoparticles. The mixtures were sonicated for 15 min and then magnetically stirred overnight in a glovebox. Finally, surface-modified copper nanoparticles were washed by centrifugation at 7500 rpm for 5 min. Another 7 mL of ethanol was added to each vial, and the solution was centrifuged again. The nanoparticles were finally dispersed in 6 mL of ethanol after being washed three times.

Controlled Oxidation of Copper Nanoparticles. The concentrations of surface-modified copper nanoparticles were determined by atomic absorption spectrometry, after which all samples were diluted to 500 μg/mL. One milliliter of surface-modified copper nanoparticles was exposed to air in an open vial under ambient conditions for 20 h. For the as-synthesized copper nanoparticles made with oleylamine, several oxidation time points were included (30 min, 2 h, 5 h, 1 day, 5 days, and 17 days) for oxidation observations.

UV−Vis Adsorption Study. UV−vis spectra of surface-modified copper nanoparticles were recorded for the range between 300 and 1000 nm at a scanning rate of 3 nm/s. To study the decrease of SPR intensity of surface-modified copper nanoparticles, we used dry compressed air bubbled through the dispersions of copper samples at a rate of 15.5 cm^3/min. The UV−vis spectrum was taken every 5 min until the reaction reached 35 min.

Reactive Oxygen Species (ROS) Assays. The ability of surface-modified copper nanoparticles to generate ROS in solution was measured using a fluorescent dye (2,7-dichlorodihydrofluorescein diacetate, DCFH-DA) and a spectrofluorometer (absorbance maximum, 485 nm; emission maximum, 535 nm). Our protocol for ROS assay is modified from that described by Dr. Philip Hopke *et al.*[42] We showed in previous studies that our acellular ROS results are consistent with results from electron spin resonance (EPR) spectroscopy and also correlate with cellular oxidative stress and *in vivo* lung inflammation following bolus respiratory tract delivery of nanoparticles,[9] all of which demonstrated the reliability of the ROS assay as a screening tool. In order to cleave the acetate group from the dye, 20 mL of sodium hydroxide (0.01 N) was added to 500 μL of DCFH-DA (5 mM) and the mixture was incubated at room temperature in a dark bottle for 30 min. Then 100 mL of sodium phosphate buffer (25 mM, pH = 7.2) was added to stop the reaction. H_2O_2 standards were made at known concentrations (0, 5, 10, 20, 30, 40, 60, 80 μM, R^2 = 0.995). The standards (100 μL) or copper particle suspensions (10−150 μL) in sodium phosphate buffer (0.05 mg/mL) were added to test tubes. Sodium phosphate buffer (10−200 μL) was used as the blank. Right before use, 1 mL of horseradish peroxidase (HRP, 2.2 U/mL) was added to the DCFH/NaOH/PBS mixture to enhance the oxidation of DCFH; no fluorescent signal can be measured if HRP is absent from the reaction.[14] In a dark room, 3 mL of DCFH/HRP mixture was added to each tube of the standards, copper samples, and blanks, which were then incubated in a 37 °C water bath for 15 min before the measurement of fluorescent intensity. The level of ROS generated by surface-modified copper nanoparticles was expressed as equivalent [H_2O_2], and the results were obtained by subtracting the readings of blank samples from the measured values of copper samples. Calibrations of the H_2O_2 standards and readings of the blanks are shown in Figure S4. The standards show good linear response, and the blanks have negligible background signal.

Characterizations. Transmission electron microscopy (TEM) and high-resolution TEM (HR-TEM) were used to characterize the copper nanoparticles. The images were taken on an FEI TECNAI F-20 field emission microscope at an accelerating voltage of 200 keV. Powder X-ray diffraction (PXRD) patterns were recorded using a Philips MPD diffractometer with a Cu Kα X-ray source (λ = 1.5405 Å). Attenuated total reflectance infrared spectra (ATR-IR) were collected on a Shimadzu FTIR-8400S spectrophotometer with a MIRacle ATR accessory. The concentrations of surface-modified copper nanoparticles were determined by atomic absorption spectrometry measurements. Copper nanoparticles were dispersed in 6 mL of ethanol after surface modifications. One milliliter of each sample was dried completely and then dissolved in concentrated nitric acid. The samples were further diluted with 2% nitric acid and their Cu content measured using Perkin-Elmer AAnalyst 600 atomic absorption spectrophotometer. The copper concentrations were obtained by regression analysis compared to known copper standards.

Conflict of Interest: The authors declare no competing financial interest.

Acknowledgment. We thank P. Mercer and R. Gelein for their valuable technical assistance. This work was supported by National Institutes of Health grant R01 CA134218 (AE) and an Environmental Health Sciences Center grant (ES01247). It made use of Shared Facilities at University of Rochester River Campus EM Lab.

Supporting Information Available: ATR-IR spectra of pure oleylamine and mercaptocarboxylic acids (Figure S1), UV−vis spectra (Figure S2), HR-TEM of oxidized Cu-MDA and Cu-MHA (Figure S3), and calibration of H_2O_2 standards and blanks (Figure S4). This material is available free of charge *via* the Internet at http://pubs.acs.org.

REFERENCES AND NOTES

1. Landsiedel, R.; Ma-Hock, L.; Kroll, A.; Hahn, D.; Schnekenburger, J.; Wiench, K.; Wohlleben, W. Testing Metal-Oxide Nanomaterials for Human Safety. *Adv. Mater.* **2010**, *22*, 2601–2627.
2. Oberdorster, G.; Oberdorster, E.; Oberdorster, J. Nanotoxicology: An Emerging Discipline Evolving from Studies of Ultrafine Particles. *Environ. Health Perspect.* **2005**, *113*, 823–839.
3. Oberdorster, G.; Stone, V.; Donaldson, K. Toxicology of Nanoparticles: A Historical Perspective. *Nanotoxicology* **2007**, *1*, 2–25.
4. Xia, T.; Kovochich, M.; Liong, M.; Madler, L.; Gilbert, B.; Shi, H. B.; Yeh, J. I.; Zink, J. I.; Nel, A. E. Comparison of the Mechanism of Toxicity of Zinc Oxide and Cerium Oxide Nanoparticles Based on Dissolution and Oxidative Stress Properties. *ACS Nano* **2008**, *2*, 2121–2134.
5. Zhu, S. Q.; Oberdorster, E.; Haasch, M. L. Toxicity of an Engineered Nanoparticle (Fullerene, C-60) in Two Aquatic Species, Daphnia and Fathead Minnow. *Mar. Environ. Res.* **2006**, *62*, S5–S9.
6. Kasemets, K.; Ivask, A.; Dubourguier, H. C.; Kahru, A. Toxicity of Nanoparticles of ZnO, CuO and TiO_2 to Yeast *Saccharomyces cerevisiae*. *Toxicol. in Vitro* **2009**, *23*, 1116–1122.
7. Wiench, K.; Wohlleben, W.; Hisgen, V.; Radke, K.; Salinas, E.; Zok, S.; Landsiedel, R. Acute and Chronic Effects of Nano- and Non-nano-scale TiO_2 and ZnO Particles on Mobility and Reproduction of the Freshwater Invertebrate Daphnia Magna. *Chemosphere* **2009**, *76*, 1356–1365.
8. Karlsson, H. L.; Cronholm, P.; Gustafsson, J.; Moller, L. Copper Oxide Nanoparticles Are Highly Toxic: A Comparison between Metal Oxide Nanoparticles and Carbon Nanotubes. *Chem. Res. Toxicol.* **2008**, *21*, 1726–1732.
9. Rushton, E. K.; Jiang, J.; Leonard, S. S.; Eberly, S.; Castranova, V.; Biswas, P.; Elder, A.; Han, X. L.; Gelein, R.; Finkelstein, J.; *et al.* Concept of Assessing Nanoparticle Hazards Considering Nanoparticle Dosemetris and Chemical/Bilogical Response Metrics. *J. Toxicol. Environ. Health, Part A* **2010**, *73*, 445–461.

10. Vanwinkle, B. A.; Bentley, K. L. D.; Malecki, J. M.; Gunter, K. K.; Evans, I. M.; Elder, A.; Finkelstein, J. N.; Oberdorster, G.; Gunter, T. E. Nanoparticle (NP) Uptake by Type I Alveolar Epithelial Cells and Their Oxidant Stress Response. *Nanotoxicology* **2009**, *3*, 307–318.
11. Andersson, P. O; Lejon, C.; Hammarstrom, B. E.; Akfur, C.; Linnea, A.; Bucht, A.; Osterlund, L. Polymorph- and Size-Dependent Uptake and Toxicity of TiO_2 Nanoparticles in Living Lung Epithelial Cells. *Small* **2011**, *7*, 514–523.
12. Elder, A.; Gelein, R.; Silva, V.; Feikert, T.; Opanashuk, L.; Carter, J.; Potter, R.; Maynard, A.; Finkelstein, J.; Oberdorster, G. Translocation of Inhaled Ultrafine Manganese Oxide Particles to the Central Nervous System. *Environ. Health Perspect.* **2006**, *114*, 1172–1178.
13. Santhanam, P.; Wagner, J. G.; Elder, A.; Gelein, R.; Carter, J. M.; Driscoll, K. E.; Oberdorster, G.; Harkema, J. R. Effects of Subchronic Inhalation Exposure to Carbon Black Nanoparticles in the Nasal Airways of Laboratory Rats. *Int. J. Nanotechnol.* **2008**, *5*, 30–54.
14. Gillespie, P. A.; Kang, G. S.; Elder, A.; Gelein, R.; Chen, L.; Moreira, A. L.; Koberstein, J.; Tchou-Wong, K. M.; Gordon, T.; Chen, L. C. Pulmonary Response after Exposure to Inhaled Nickel Hydroxide Nanoparticles: Short and Long-Term Studies in Mice. *Nanotoxicology* **2010**, *4*, 106–119.
15. Kocbek, P.; Teskac, K.; Kreft, M. E.; Kristl, J. Toxicological Aspects of Long-Term Treatment of Keratinocytes with ZnO and TiO_2 Nanoparticles. *Small* **2010**, *6*, 1908–1917.
16. Lanone, S.; Rogerieux, F.; Geys, J.; Dupont, A.; Maillot-Marechal, E.; Boczkowski, J.; Lacroix, G.; Hoet, P. Comparative Toxicity of 24 Manufactured Nanoparticles in Human Alveolar Epithelial and Macrophage Cell Lines. *Part. Fibre Toxicol.* **2009**, *6*, DOI: 10.1186/1743-8977-6-14.
17. Cioffi, N.; Ditaranto, N.; Torsi, L.; Picca, R. A.; De Giglio, E.; Sabbatini, L.; Novello, L.; Tantillo, G.; Bleve-Zacheo, T.; Zambonin, P. G. Synthesis, Analytical Characterization and Bioactivity of Ag and Cu Nanoparticles Embedded in Poly-vinyl-methyl-ketone Films. *Anal. Bioanal. Chem.* **2005**, *382*, 1912–1918.
18. Wei, Y. H.; Chen, S.; Kowalczyk, B.; Huda, S.; Gray, T. P.; Grzybowski, B. A. Synthesis of Stable, Low-Dispersity Copper Nanoparticles and Nanorods and Their Antifungal and Catalytic Properties. *J. Phys. Chem. C* **2010**, *114*, 15612–15616.
19. Anyaogu, K. C.; Fedorov, A. V.; Neckers, D. C. Synthesis, Characterization, and Antifouling Potential of Functionalized Copper Nanoparticles. *Langmuir* **2008**, *24*, 4340–4346.
20. Rakhmetova, A. A.; Alekseeva, T. P.; Bogoslovskaya, O. A.; Leipunskii, I. O.; Ol'khovskaya, I. P.; Zhigach, A. N.; Glushchenko, N. N. Wound-Healing Properties of Copper Nanoparticles as a Function of Physicochemical Parameters. *Nanotechnologies in Russia* **2010**, *5*, 271–276.
21. Fahmy, B.; Cormier, S. A. Copper Oxide Nanoparticles Induce Oxidative Stress and Cytotoxicity in Airway Epithelial Cells. *Toxicol. in Vitro* **2009**, *23*, 1365–1371.
22. Midander, M.; Cronholm, P.; Karlsson, H. L.; Elihn, K.; Moller, L.; Leygraf, C.; Wallinder, I. O. Surface Characteristics, Copper Release, and Toxicity of Nano- and Micrometer-Sized Copper and Copper(II) Oxide Particles: A Cross-Disciplinary Study. *Small* **2009**, *5*, 389–399.
23. Chompoosor, A.; Saha, K.; Ghosh, P. S.; Macarthy, D. J.; Miranda, O. R.; Zhu, Z. J.; Arcaro, K. F.; Rotello, V. M. The Role of Surface Functionality on Acute Cytotoxicity, ROS Generation and DNA Damage by Cationic Gold Nanoparticles. *Small* **2010**, *6*, 2246–2249.
24. Zhu, Z. J.; Carboni, R.; Quercio, M. J.; Yan, B.; Miranda, O. R.; Anderton, D. L.; Arcaro, K. F.; Rotello, V. M.; Vachet, R. W. Surface Properties Dictate Uptake, Distribution, Excretion, and Toxicity of Nanoparticles in Fish. *Small* **2010**, *6*, 2261–2265.
25. Wang, J.; Gong, J.; Xiong, Y.; Yang, J.; Gao, Y.; Liu, Y.; Lu, X.; Tang, Z. Shape-Dependent Electrocatalytic Activity of Monodispersed Gold Nanocrystals toward Glucose Oxidation. *Chem. Commun.* **2011**, *47*, 6894–6896.
26. Bagaria, H. G.; Ada, E. T.; Shamsuzzoha, M.; Nikles, D. E.; Johnson, D. T. Understanding Mercapto Ligand Exchange on the Surface of FePt Nanoparticles. *Langmuir* **2006**, *22*, 7732–7737.
27. Wijaya, A.; Hamad-Schifferli, K. Ligand Customization and DNA Functionalization of Gold Nanorods *via* Round-Trip Phase Transfer Ligand Exchange. *Langmuir* **2008**, *24*, 9966–9969.
28. Yano, K.; Nandwana, V.; Chaubey, G. S.; Poudyal, N.; Kang, S.; Arami, H.; Griffis, J.; Liu, J. P. Synthesis and Characterization of Magnetic FePt/Au Core/Shell Nanoparticles. *J. Phys. Chem. C* **2009**, *113*, 13088–13091.
29. Shukla, N.; Liu, C.; Jones, P. M.; Weller, D. FTIR Study of Surfactant Bonding to FePt Nanoparticles. *J. Magn. Magn. Mater.* **2003**, *266*, 178–184.
30. Elder, A.; Yang, H.; Gwiazda, R.; Teng, X.; Thurston, S.; He, H.; Oberdorster, G. Testing Nanomaterials of Unknown Toxicity: An Example Based on Platinum Nanoparticles of Different Shapes. *Adv. Mater.* **2007**, *19*, 3124–3129.
31. Yanase, A.; Komiyama, H. *In Situ* Observation of Oxidation and Reduction of Small Supported Copper Particles Using Optical-Absorption and X-ray Diffraction. *Surf. Sci.* **1991**, *248*, 11–19.
32. Kanninen, P.; Johans, C.; Merta, J.; Kontturi, K. Influence of Ligand Structure on the Stability and Oxidation of Copper Nanoparticles. *J. Colloid Interface Sci.* **2008**, *318*, 88–95.
33. Cabrera, N.; Mott, N. F. Theory of the Oxidation of Metals. *Rep. Prog. Phys.* **1949**, *12*, 163–184.
34. Kim, J. H.; Ehrman, S. H.; Germer, T. A. Influence of Particle Oxide Coating on Light Scattering by Submicron Metal Particles on Silicon Wafers. *Appl. Phys. Lett.* **2004**, *84*, 1278–1280.
35. Chan, G. H.; Zhao, J.; Hicks, E. M.; Schatz, G. C.; Van Duyne, R. P. Plasmonic Properties of Copper Nanoparticles Fabricated by Nanosphere Lithography. *Nano Lett.* **2007**, *7*, 1947–1952.
36. Hung, L. I.; Tsung, C. K.; Huang, W. Y.; Yang, P. D. Room-Temperature Formation of Hollow Cu_2O Nanoparticles. *Adv. Mater.* **2010**, *22*, 1910–1915.
37. Pedersen, D. B.; Wang, S. L.; Liang, S. H. Charge-Transfer-Driven Diffusion Processes in Cu@Cu-Oxide Core−Shell Nanoparticles: Oxidation of 3.0 ± 0.3 nm Diameter Copper Nanoparticles. *J. Phys. Chem. C* **2008**, *112*, 8819–8826.
38. Lisiecki, I.; Billoudet, F.; Pileni, M. P. Control of the Shape and the Size of Copper Metallic Particles. *J. Phys. Chem.* **1996**, *100*, 4160–4166.
39. Borgohain, K.; Murase, N.; Mahamuni, S. Synthesis and Properties of Cu_2O Quantum Particles. *J. Appl. Phys.* **2002**, *92*, 1292–1297.
40. Yin, M.; Wu, C. K.; Lou, Y. B.; Burda, C.; Koberstein, J. T.; Zhu, Y. M.; O'Brien, S. Copper Oxide Nanocrystals. *J. Am. Chem. Soc.* **2005**, *127*, 9506–9511.
41. Son, S. U.; Park, I. K.; Park, J.; Hyeon, T. Synthesis of Cu_2O Coated Cu Nanoparticles and Their Successful Applications to Ullmann-Type Amination Coupling Rreactions of Aryl Chlorides. *Chem. Commun.* **2004**, *7*, 778–779.
42. Venkatachari, P.; Hopke, P. K.; Grover, B. D.; Eatough, D. J. Measurement of Particle-Bound Reactive Oxygen Species in Rubidoux Aerosols. *J. Atmos. Chem.* **2005**, *50*, 49–58.